



This is a repository copy of *Predicting the energy storage density in poly(methyl methacrylate)/methyl ammonium lead iodide composites*.

White Rose Research Online URL for this paper:
<http://eprints.whiterose.ac.uk/147300/>

Version: Accepted Version

Article:

Kennedy, C.D., Sinclair, D.C. orcid.org/0000-0002-8031-7678, Reaney, I.M. orcid.org/0000-0003-3893-6544 et al. (1 more author) (2019) Predicting the energy storage density in poly(methyl methacrylate)/methyl ammonium lead iodide composites. *Journal of Applied Physics*, 125 (21). 214103. ISSN 0021-8979

<https://doi.org/10.1063/1.5083799>

This article may be downloaded for personal use only. Any other use requires prior permission of the author and AIP Publishing. The following article appeared in *Journal of Applied Physics* 125, 214103 (2019) and may be found at <https://doi.org/10.1063/1.5083799>.

Reuse

Items deposited in White Rose Research Online are protected by copyright, with all rights reserved unless indicated otherwise. They may be downloaded and/or printed for private study, or other acts as permitted by national copyright laws. The publisher or other rights holders may allow further reproduction and re-use of the full text version. This is indicated by the licence information on the White Rose Research Online record for the item.

Takedown

If you consider content in White Rose Research Online to be in breach of UK law, please notify us by emailing eprints@whiterose.ac.uk including the URL of the record and the reason for the withdrawal request.



eprints@whiterose.ac.uk
<https://eprints.whiterose.ac.uk/>

C.D. Kennedy ^{a)}, D.C. Sinclair, I.M. Reaney and J.S. Dean

Department of Materials Science and Engineering, University of Sheffield, Sheffield, S1 3JD, United Kingdom

In high energy density pulsed power capacitors high permittivity particles are dispersed within a high breakdown strength polymer matrix. In theory such composites should be able to achieve higher volumetric energy densities than is possible with either of the individual constituents. $\text{CH}_3\text{NH}_3\text{PbI}_3$ (MALI) has a perovskite structure and may be fabricated at room temperature using a mechano-synthesis route in ethanol. In this study, MALI is used for the first time to form a dielectric composite. Poly(methyl methacrylate) (PMMA) is used as the matrix. Theoretical models are used to predict composite permittivity values that are compared to experimental values. Finite Element modelling (FEM) is used to simulate their effective permittivity, and beyond what the theoretical models can achieve, predicts their energy storage capabilities by analyzing electric field intensification. The simulations show increasing energy storage capability with penetration of MALI but this is limited experimentally by their mixing capability.

I. INTRODUCTION

There is an increasing demand for high energy density capacitors to meet the larger power delivery required by applications such as electric vehicles ¹⁻³. The introduction of high permittivity inorganic particles, such as BaTiO_3 , into a polymer matrix is a common way to increase the relative permittivity (ϵ_r) of the resulting composite ⁴⁻⁶. However, the homogenous distribution of particles due to the high surface energy and mechanical instability, brought about by the weak adhesion between inorganic particles and the polymer matrix, are challenging issues to overcome ^{7,8}. Surface modifications of these materials can help overcome some of these problems but ultimately results in lower ϵ_r ^{9,10}.

Due to its unique optoelectronic properties, such as narrow bandgap and high density of moderately high mobility charge carriers, $\text{CH}_3\text{NH}_3\text{PbI}_3$ (MALI) has caused a disruptive change in the development of solar cells ^{11,12} but its high intrinsic permittivity ($\epsilon_r = 62$) and simple fabrication at room temperature ¹³ suggest that it is also a promising candidate as a distributed particulate to enhance ϵ_r of polymer composites and has not been explored before.

Finite element methods (FEM) have previously been used to study the effect of microstructural changes on the ϵ_r and electric field in functional oxides and composite materials ¹⁴⁻¹⁹. An *in-house* finite element package, Elcer, has been developed which

^{a)} Author to whom correspondence should be addressed. Electronic mail: cdkenne1978@gmail.com.

solves Maxwell's equations in 3D and time for a known geometry¹⁶⁻¹⁸ and has been used to study composite materials as well as the effect of porosity in ceramics²⁰. In the latter it was found that while two-dimensional simulations can provide insight, a full 3D model is required to represent the geometry of composites^{21,22}, resulting in a better prediction of the electrical response. In this work MALI/PMMA composites are simulated using experimentally derived properties and fully 3D microstructures. Simulated electrical responses are compared to predictions from theoretical models and experimental data to guide the design and optimisation of composites, thereby providing a cheaper and faster route to optimisation than material intensive trial and error by experimentation.

A. Theoretical models

Many theoretical models have been developed to study dielectric-polymer composites, mainly derived from effective medium theory²³, which predicts the dielectric permittivity of composite materials. A limitation of this approach is that the underlying microstructure is not considered. The simplest of these models only considers ϵ_r of the constituent materials, whereas others include the morphology and dispersion of particles, and the interaction between the two materials. A summary of these models can be found in refs^{1,3,24}. These predictions often fail for higher loadings of filler where the interaction between particles is important²¹.

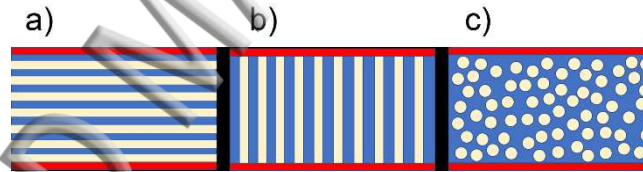


FIG. 1. Schematic of series, parallel and composite geometries, (a), (b), and (c) respectively, with red indicating the electrical contacts.

One commonly used approach is the Lichtenecker mixing rule²⁵, developed from the theoretical Wiener boundary values²⁶ of a series and parallel model, as shown in equations (1) and (2) (see FIG. 1):

series model (lower limit),

$$\epsilon_r = \frac{\epsilon_m \epsilon_f}{\epsilon_m v_f + \epsilon_f (1 - v_f)} \quad (1)$$

parallel model (upper limit),

$$\varepsilon_r = (1 - v_f)\varepsilon_m + v_f\varepsilon_f \quad (2)$$

where ε_r , ε_f and ε_m are the relative permittivities of the composite, filler and matrix, respectively and v_f is the volume fraction of filler. These series and parallel formulations are representative of the lower and upper limits of the composite permittivity of Lichtenecker's formulae which has been shown to have theoretical foundations in the effective medium theory²⁶:

$$\varepsilon_r^\alpha = (1 - v_f)\varepsilon_m^\alpha + v_f\varepsilon_f^\alpha \quad (3)$$

where α is defined as a topological factor which can vary from -1 to 1. When $\alpha = 1$ and -1 , equation (3) reduces to a series layer (1) and purely parallel (2) formulation, respectively, but it is unclear how to determine the topological factor for prediction of ε_r . Thus, α is used to understand the topology of an experimental set of samples. The Lichtenecker formula has also been shown to fit well for low v_f if ε_r of the materials is of similar magnitude⁸. Bruggeman developed a mean field theory,

$$(1 - v_f) \frac{\varepsilon_m - \varepsilon_r}{(\varepsilon_m + 2\varepsilon_r)} + v_f \frac{\varepsilon_f - \varepsilon_r}{(\varepsilon_f + 2\varepsilon_r)} = 0 \quad (4)$$

in which the composite is treated as repeated unit cells with each unit consisting of a matrix phase with a spherical inclusion at the centre.

B. Dielectric breakdown strength

The dielectric breakdown strength is a statistical representation of the maximum electric field which a dielectric material can withstand before losing its insulating capability. For linear dielectric materials, the energy storage density is quadratically dependent on the magnitude of the applied electric field:

$$U = \frac{1}{2} \varepsilon_0 \varepsilon_r E^2 \quad (5)$$

where U is the energy storage density, ε_0 is the permittivity of free space, and E is the magnitude of the applied electric field. The maximum energy which can be stored in a dielectric material then is determined by both ε_r and breakdown strength which

defines the maximum limit of the electric field that can be generated in the material. Thus, the electrical breakdown strength is an important parameter to consider when choosing a suitable dielectric material.

Various approaches have been adopted to model the breakdown strength of composite materials such as the phase field method which is analogous to studying the fracture of solids²⁷⁻²⁹. A semi-empirical approach has also been taken¹⁵ to correlate probability density functions of the electric field vector magnitudes in simulations with experimental electrical breakdown data. A critical intensification factor that is inversely proportional to the electrical breakdown strength was introduced to indicate its reduction relative to the pure polymer such that:

$$E_{bd}^c = \frac{E_{bd}^m}{I_c} \quad (6)$$

where I_c is the critical intensification factor, and E_{bd}^c and E_{bd}^m are the composite and polymer matrix electrical breakdown strengths, respectively. Wang et. al. reported that using an upper boundary of 30% of electric field vector magnitudes from finite element analysis fit well with their experimental breakdown strength also verified with data found in the literature¹⁵. This approach is analogous to that taken in the Fröhlich high-energy criterion³⁰ where it is the high tail end of electron energies that propagates breakdown instead of the high tail end of the magnitudes of the electric field vector here. An increased electric field therefore could result in a greater number of high energy electrons which can lead to impact ionization, possibly initiating electrical breakdown.

II. EXPERIMENTAL METHODS

To provide experimental data for use as direct input into the FEM simulations (electrical properties, microstructural features), MALI (99%) - PMMA (average $M_w \sim 15,000$ by GPC) composites were fabricated.

PMMA was obtained from Sigma Aldrich and used as received. MALI was fabricated using a mechanosynthesis route. Stoichiometric proportions of $\text{CH}_3\text{NH}_3\text{I}$ (+5wt% excess) and PbI_2 were added to 100 ml of dry ethanol and ball milled for 1 hour. The resulting mixture was dried overnight in an oven at 90 °C and X-ray Diffraction (XRD) of the powder at room temperature showed the presence of the perovskite phase MALI with no traces of any secondary phase.

To fabricate PMMA-MALI composites, PMMA was dissolved in a mixture of toluene and ethanol (molar 52:48 respectively), MALI powder was added and the solution mixed with an overhead stirrer (300 rpm) for 2-3 hours until the composite:solvent ratio reached $\sim 2:3$. The viscous solution was then sonicated for 30 minutes and poured into a 10 mm disc

mould to dry in air. The composite disc was then uniaxially hot pressed with 0.5 ton pressure at 100 °C and allowed to cool to room temperature in the press. Filler was limited to 35% due to mixing limitations with the polymer. As particle size decreases the surface area onto which the polymer matrix adsorbs increases. As a result, there is a limit on maximum v_f which can be achieved whilst maintaining mechanical stability and minimal porosity. Beyond this critical v_f the dispersion of filler is poor due to agglomeration.

X-ray diffraction was performed on the constituent materials and the resulting composite using a D2-phaser over a 2θ range of 10° - 60° with a scanning speed of 6°/min and step size 0.02° using CuK α radiation ($\lambda = 1.5418 \text{ \AA}$). Particle size (Malvern Mastersizer 3000) analysis was performed on MALI using the dry powder dispersion method by laser diffraction. The composite samples were mounted on Al stubs with Ag paste and sputter coated with Au to enable back scattered images of the polished surfaces to be obtained using SEM (FEI Inspect F, JEOL). To enable dielectric measurements, gold electrodes were sputter coated onto both sides of the sample. The dielectric properties of the samples were obtained using a precision LCR meter (Agilent E4980A) at room temperature with measurements taken with frequency going from 20 Hz to 1MHz.

III. EXPERIMENTAL RESULTS

A. Scanning electron microscopy

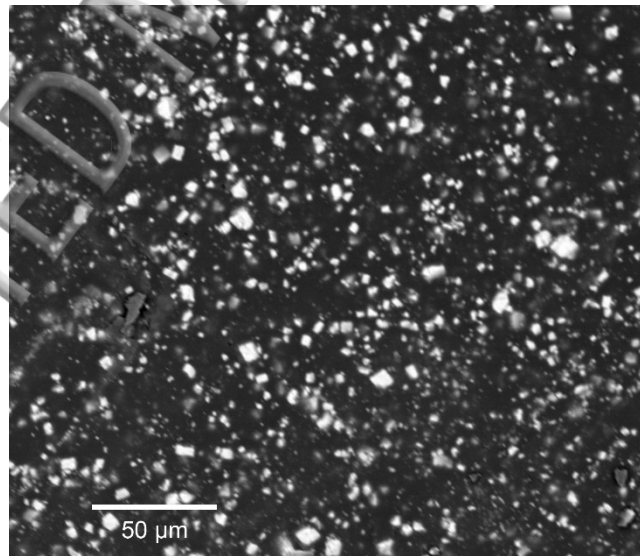


FIG. 2. Back scattered electron image of a 20% v_f PMMA/MALI composite. The denser MALI particles (white) are easily distinguishable and well dispersed.

SEM was carried out on a 20% v_f MALI in PMMA composite. Due to the higher atomic weight of PbI_2 the signal from MALI is much stronger than that from PMMA so that it is easy to distinguish between them. A good dispersion of particles and minimal agglomeration can be observed in FIG. 2

B. Particle size analysis

Particle size distribution analysis of the MALI powder revealed a peak volume density for a particle size 7.2 μm , FIG. 2. Approximately 64% of particles are in the range of $\sim 1\text{-}11$ μm and over 98% are between $\sim 0.6\text{-}12$ μm . Also shown is the particle size distribution found by analysing SEM images of MALI in PMMA composites. This was carried out using MATLAB image processing function regionprops and making corrections to account for the 2D projection of a slice through a 3D geometry, with the assumption of spherical particles with a log normal distribution of sizes^{31,32}. The deviation of the right side tail is due to the difficulty of properly characterizing it from a relatively small sample set of values from what is a widely dispersed population³².

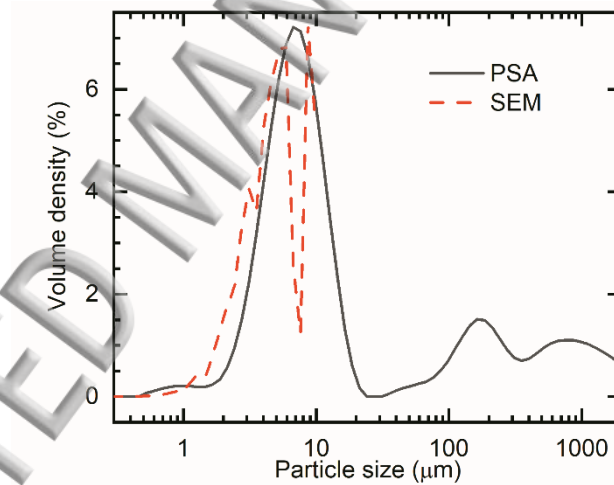


FIG. 3. Particle size analysis of MALI powder using a Malvern Mastersizer 3000 (black solid line). A volume density peak of 7.2 μm was established when considering the number of particles in each size class. Also shown is particle size distribution calculated analyzing SEM images of MALI in PMMA composite (red dashed line).

C. X-ray diffraction

XRD patterns of MALI, PMMA and PMMA-MALI composites are shown FIG. 3. As PMMA is amorphous it shows a broad background trace with no sharp peaks whereas all peaks in the MALI trace are attributed to a tetragonal perovskite cell.

The PMMA-MALI composite shows no additional features, suggesting the MALI has not reacted with the PMMA or solvents to produce any additional crystalline phases. This allows us to replicate the microstructure of the composite as distinct regions of the individual materials.

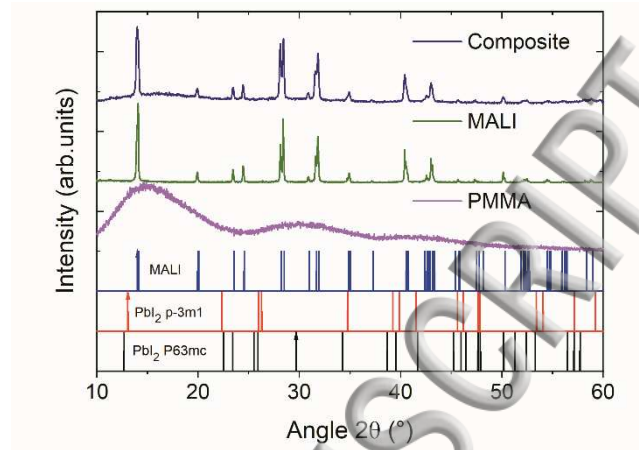


FIG. 4. (top three traces) XRD patterns for PMMA, MALI and PMMA/MALI composites at room temperature. The patterns show MALI has not decomposed during processing with PMMA hence unwanted contamination is not present in the composites. (bottom three traces) Theoretical XRD peak positions for MALI and two forms of PbI_2 at room temperature. Comparison of these traces with the observed pattern for MALI powder (green trace) shows the powder to be single-phase and free from PbI_2 .

D. Dielectric properties

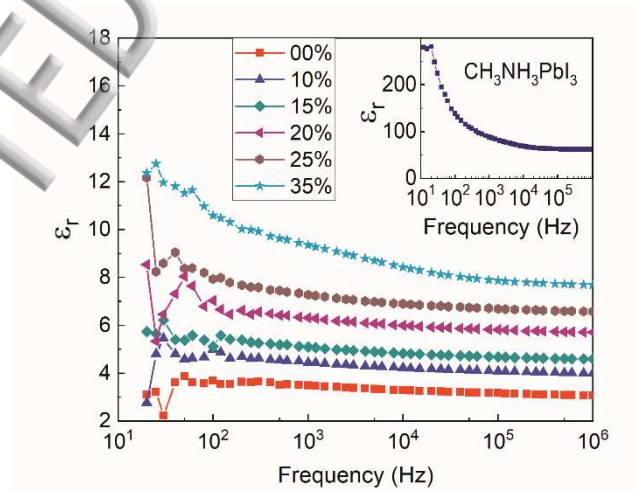


FIG. 5. Frequency dependence of the relative permittivity of PMMA-MALI composites with varying v_f of MALI. Inset shows frequency dependence of the permittivity of MALI.

To extract the electrical properties, room temperature complex impedance, Z^* plots were fitted with a single RC element to extract the bulk conductivity (σ) and relative permittivity of MALI and gave values of $\sigma = 0.3 \mu S \cdot cm^{-1}$ and $\epsilon_r = 62$, respectively. The room temperature ϵ_r of the composites with measurements taken with frequency going from 20 Hz to 1 MHz for various v_f of MALI (see FIG. 4). PMMA shows an almost flat frequency dependence with $\epsilon_r \sim 3$.

As the v_f of MALI increases the low frequency permittivity shows a further enhancement when compared to the higher frequency data. MALI shows a flat profile in ϵ_r (62) over the high frequency range 10 kHz -1MHz. As the frequency decreases more polarization mechanisms become active and the permittivity increases steadily to ~ 140 at 100 Hz. Below this frequency the permittivity increases sharply which is attributed to free charge carriers migrating to the sample-electrode interfaces.

IV. THEORETICAL MODEL PREDICTIONS

Using our experimental data, we now look to compare FEM to analytical and semi-analytical approaches for predicting this systems permittivity. The extracted permittivities of PMMA and MALI and their v_f were used as input parameters in commonly used theoretical models ^{1,3,24}. Least squares fitting along with the coefficient of determination (goodness of fit), R^2 , values were obtained for each model for the PMMA-MALI composites. Some theoretical models have been discounted (e.g. Rayleigh ³³, Maxwell-Garnet ³⁴, Maxwell-Wagner ³⁵) as they gave very poor fits to the data with R^2 approximating zero. To simulate the effect of the physical microstructure of the two materials on the electrical properties of the composite an in-house FEM package, ELCer, is used to predict the electrical response of the system ¹⁶⁻¹⁸.

A. Optimization of energy storage

In the PMMA/MALI composites, there are many interacting particles. To represent this, we generated a 3D geometry for 28 different v_f . Each system contained an agglomeration-free distribution of spherical particles with diameter $7.2 \mu m$ and v_f of filler between 0.82 and 37.6%, see example in FIG. 7 (a) and (b). To mimic a random dispersion, a sequential addition method was used ^{15,36}. This method added particles one at a time but is limited in v_f due to large voids generated between particles within which another particle cannot fit. To overcome this limitation, we coupled this approach with an underlying structure of a hexagonal close packed (HCP) lattice.

First, a series of HCP sites are generated as placement points. The sequential method is then used to place a particle around each point constrained by a distance ($7.2 \mu m$) in each direction (see FIG. 6). This distance was chosen to ensure a good dispersion of particles but also allowed a higher packing fraction to be achieved as compared to just a random placement. No

particles were permitted to touch or overlap with each other or the external surfaces of the model. This method allowed much higher ν_f to be generated whilst still maintaining an effective randomised structure.

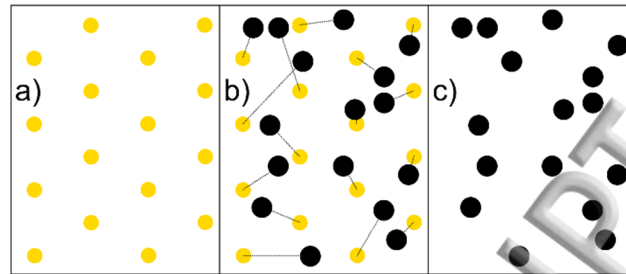


FIG. 6. Simplified 2D illustration of using an HCP structure as the basis for random placement of particles. (a) HCP co-ordinates (yellow), (b) placement of particles (black) around each co-ordinate, and (c) resultant random placement of particles.

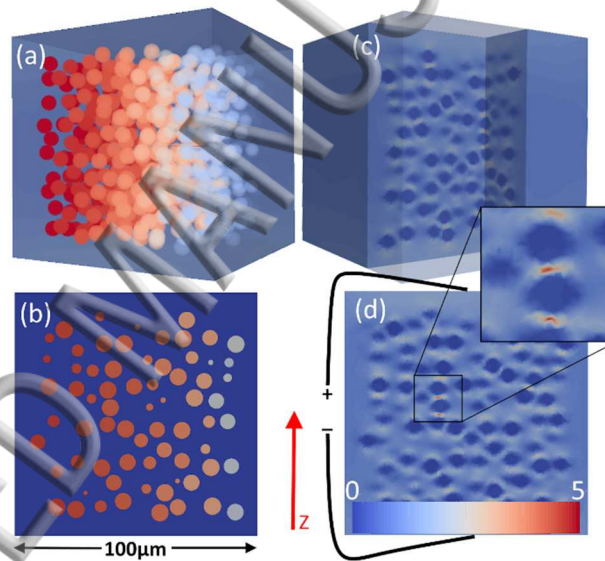


FIG. 7. Representations of 20% ν_f MALI, particle radius = 3.6 μm , dispersed in polymer with (a) and (b) showing 3D and 2D geometry, respectively. (c) and (d) 3D and 2D electric field plots, respectively, with inset showing intensified electric field (scale bar shows relative field magnitude from blue (low) to high (red)). A potential difference of 1V is applied across the sample, parallel to the z axis.

Experimental it was also found that at high volume fractions, effects such as agglomeration also was present. To observe the significant of this on the energy storage we incorporate a simple addition to these models. Using the random sequential addition method^{15,36} we now allow particles to merge. This is determined by the following process. We randomly allocate a particle into space. If no particle is present, this placement is allowed. If the placement overlaps with a current particle, the

particle present is increased to combine their volumes, with the larger spherical particle located at their centre of mass. To avoid agglomerations preferentially forming towards those first formed a maximum particle radius is imposed of $9.7\mu\text{m}$. This is chosen from experimental observations that during mixing larger agglomerations will break up. We find that the fraction of particles agglomerating increased linearly up to $\sim 70\%$ at $15\% v_f$ and then increased slowly to 85% at $40\% v_f$.

The electrical (impedance) response was then simulated using FEM for an alternating potential difference of 1V across the sample. The resulting effective permittivity of the composite was extracted by fitting the Debye peak observed in spectroscopic plots of the imaginary component of the electric modulus, M'' ^{16,37}, consistent with experimental methods.

To simulate the electric field, and ultimately the breakdown, the voltage was applied as a fixed value and allowed to reach steady state, as shown in FIG. 1 (c) and (d). To account for statistical variations in particle placement, each v_f was simulated 10 times, and the results averaged.

B. Comparison of theoretical models.

The resulting fits and parameters used are plotted in FIG. 8 and listed in TABLE I. A simple series or parallel model poorly describes the resulting permittivity. Mixing using the effective medium theory, equ. (3) with $\alpha = -0.12$, however suggests that the composite behaves closer in topology to that of a series rather than a parallel model. The fitting parameter α , depends on the distribution and shape of the particles and can't be predicted. This use of a fitting parameter was also required in the Lichtenecker fit and although they provided very good fits, they did not permit reliable prediction of properties. Analytical solutions for Bruggeman, Furukawa and Maxwell also achieve a relatively good fit to the effective permittivity but without the need for a fitting factor. Thus, these methods would be good for prediction.

The high frequency ϵ_r calculated by the FEM model as a function of the v_f of MALI in PMMA is also overlaid in FIG. 8 and shows that the average FEM is the third best fitting method but the best method that does not rely on a fitting parameter. This method using just the experimental properties of MALI and PMMA along with a realistic microstructure not only allows for a good fit for the resulting electrical properties but also allows the electric field within the model to be calculated: none of the other analytical models can achieve this. It is important to note here that we use a simple approximate of the structure and as such some features are not included. One such feature is an interfacial layer³⁸ between the MALI and PMMA. From our calculations, if we assume a layer of a few nanometres, this would only account for 0.25% of the total volume of the composite, and as such negligible in our calculations. One additional feature is that of including a dipole-dipole correlation effect³⁹ which

has not been considered here. However, even with our simple FEM approach we have predicted the composite permittivity well as shown in FIG. 8.

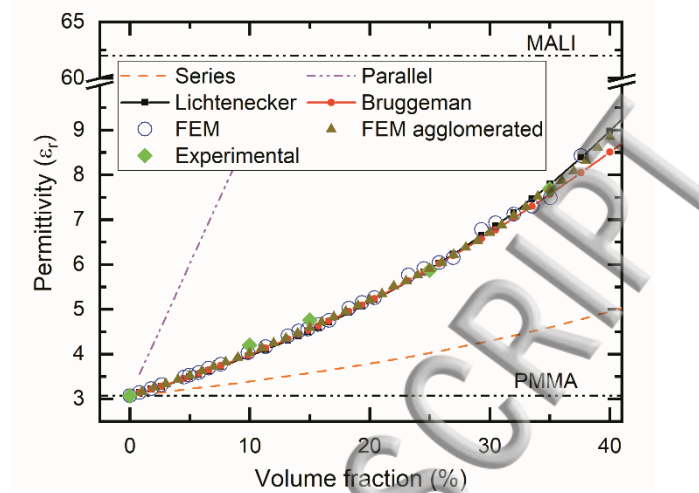


FIG. 8. Experimental and modelled high frequency ϵ_r are in good agreement. Theoretical upper (parallel) and lower (series) limits of mixing ϵ_r are indicated. The Lichtenecker model fits well with $\alpha = -0.12$ as does Bruggeman but without the use of a fitting factor. Also shown by the horizontal lines are the values of the constituent materials.

TABLE I. Goodness of fit to PMMA-MALI permittivity data for various theoretical models. Shading indicates the use of a fitting factor found using a least squares method.

Theoretical model	R ²	Fitting factor
Lichtenecker ²⁵	0.9991	-0.1232
Effective medium theory ²⁵	0.9967	0.2795
FEM	0.9943	NA
Bruggeman ⁴⁰	0.9914	NA
Furukawa ⁴¹	0.9835	NA
Maxwell ⁴⁰	0.9499	NA
Yamada ⁴²	0.8445	5.0000
Sillars ⁴³	0.6466	NA
Jaysundere–Smith ⁴⁴	0.3310	NA

C. Maximum energy storage

Using FEM, we can predict the permittivity and estimate the energy storage capability of the composites. The maximum energy storage, U_{max} , can be calculated by substituting equation (6) into (5):

$$U_{max} = \frac{1}{2} \epsilon_0 \epsilon_r \left(\frac{E_{bd}^m}{I_c} \right)^2 \quad (7)$$

FIG. 9 (a) and (b) show representative electric field magnitude histograms with critical intensification factors shown. The relative maximum field magnitudes are 4.5 and 5.1 for these 5% and 35% v_f simulations, respectively.

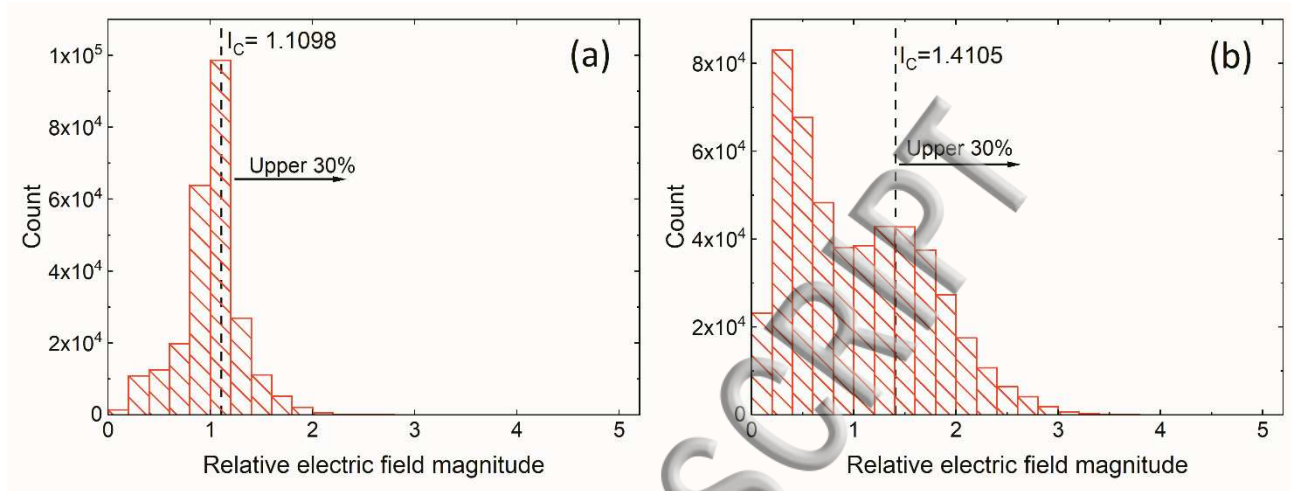


FIG. 9. Histograms for the magnitude of the electric field relative to that of the pure polymer and corresponding critical intensification factors for a (a) 5% and (b) 35% v_f .

The resulting simulated energy is plotted in FIG. 10. Small additions of MALI particles into the composite results in a lower energy storage capability. The increase in permittivity due to the introduction of the higher permittivity particles is outweighed by the resulting decrease in electrical breakdown strength. Results indicate that at least 18% v_f of MALI is needed to improve the energy storage capability of PMMA. We find that when the model includes agglomeration the permittivity of the composite is unaffected, however the breakdown strength does decrease especially at higher filler content. As such the energy storage capabilities above 20% v_f are reduced compared to the model without agglomeration as can be seen in FIG. 10. U_{max} decreases by up to 19% for a v_f of 37% MALI. This reduction can be attributed to the higher electric field stress points that are generated between the larger agglomerated particles. As such, in all cases a processing window between 18% and 35% is apparent that offers a significant increase in performance. Below 18% there is no significant increase in energy storage and above this range is not possible due to mixing capabilities. A similar trend is also found for other composite systems, not shown here, such as polystyrene / BaTiO₃ system.

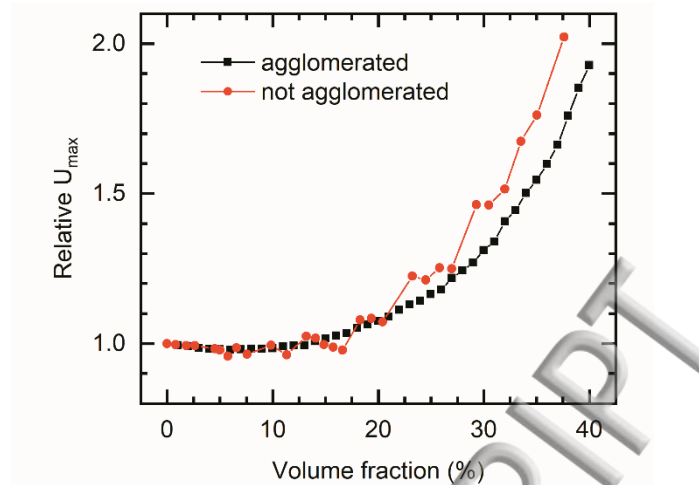


FIG. 10. Simulated maximum energy density of PMMA/MALI composites with and without agglomeration relative to pure polymer.

D. CONCLUSIONS

A finite element modelling technique has been used to predict the electrical properties of MALI-PMMA composites and estimate the optimised v_f . We have also shown that FEM is in better agreement with experimental ϵ_r results than any of the theoretical models that do not contain a fitting factor. Those models which include a fitting factor were marginally better but required the method of least squares with the experimental data present. The simulated data shows increasing energy storage capabilities of the composite with increasing v_f above 18% and is adversely affected by agglomeration, but which is limited by mixing capabilities, showing a processing window of 18% to 35% for this system.

Work is in progress with spin coating of thin MALI-PMMA films to facilitate electrical breakdown strength and energy density measurements. The FEM approach will also be further tested with other polymer/filler combinations.

ACKNOWLEDGEMENTS

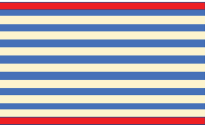
We thank the EPSRC (grant EP/L016818/1) for funding the studentship for Carl Derek Kennedy.

REFERENCES

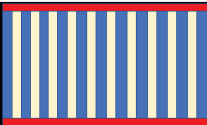
- 1 P. Barber, S. Balasubramanian, Y. Anguchamy, S. Gong, A. Wibowo, H. Gao, H. J. Ploehn, and H. C. zur Loye, *Materials* **2**, 1697 (2009).
- 2 V. K. Thakur and R. K. Gupta, *Chemical reviews* **116**, 4260 (2016).
- 3 Z. M. Dang, J. K. Yuan, J. W. Zha, T. Zhou, S. T. Li, and G. H. Hu, *Progress in Materials Science* **57**, 660 (2012).
- 4 T. Hoshina, *Journal of the Ceramic Society of Japan* **121**, 156 (2013).
- 5 B. Schumacher, H. Geßwein, J. Haußelt, and T. Hanemann, *Microelectronic Engineering* **87**, 1978 (2010).
- 6 D. Padalia, G. Bisht, U. C. Johri, and K. Asokan, *Solid State Sciences* **19**, 122 (2013).
- 7 S. Siddabattuni, T. P. Schuman, and F. Dogan, *ACS Applied Materials & Interfaces* **5**, 1917 (2013).
- 8 S. H. Liu, S. M. Xiu, B. Shen, J. W. Zhai, and L. B. Kong, *Polymers* **8**, 11 (2016).

- C. W. Beier, M. A. Cuevas, and R. L. Brutchey, *Langmuir* **26**, 5067 (2010).
- K. Yu, Y. J. Niu, Y. C. Zhou, Y. Y. Bai, and H. Wang, *Journal of the American Ceramic Society* **96**, 2519 (2013).
- M. N. F. Hoque, M. Yang, Z. Li, N. Islam, X. Pan, K. Zhu, and Z. Fan, *ACS Energy Letters*, 142 (2016).
- H. J. Snaith, *Journal of Physical Chemistry Letters* **4**, 3623 (2013).
- D. Prochowicz, M. Franckevičius, A. M. Cieślak, S. M. Zakeeruddin, M. Grätzel, and J. Lewiński, *J. Mater. Chem. A* **3**, 20772 (2015).
- V. Myroshnychenko and C. Brosseau, *Journal of Applied Physics* **97** (2005).
- Z. P. Wang, J. K. Nelson, H. Hillborg, S. Zhao, and L. S. Schadler, *Composites Science and Technology* **76**, 29 (2013).
- J. S. Dean, J. H. Harding, and D. C. Sinclair, *Journal of the American Ceramic Society* **97**, 885 (2014).
- J. P. Heath, J. S. Dean, J. H. Harding, and D. C. Sinclair, *Journal of the American Ceramic Society* **98**, 1925 (2015).
- J. S. Dean, P. Y. Foeller, I. M. Reaney, and D. C. Sinclair, *Journal of Materials Chemistry A* (2016).
- X. Zhao, Y. Wu, Z. Fan, and F. Li, *Journal of Applied Physics* **95**, 8110 (2004).
- G. Dale, M. Strawhorne, D. C. Sinclair, and J. S. Dean, *Journal of the American Ceramic Society* **101**, 1211 (2018).
- P. Kim, N. M. Doss, J. P. Tillotson, P. J. Hotchkiss, M.-J. Pan, S. R. Marder, J. Li, J. P. Calame, and J. W. Perry, *ACS Nano* **3**, 2581 (2009).
- Y. Wang, S. Kim, G. Li, and L. Sun, *Computational Materials Science* **104**, 69 (2015).
- W. R. Tinga, W. A. G. Voss, and D. F. Blossey, *Journal of Applied Physics* **44**, 3897 (1973).
- A. Jain, K. J. Prashanth, A. K. Sharma, and P. N. Rashmi, *Polymer Engineering and Science* **55**, 1589 (2015).
- Y. Rao, J. M. Qu, T. Marinis, and C. P. Wong, *Ieee Transactions on Components and Packaging Technologies* **23**, 680 (2000).
- T. Zakri, J.-P. Laurent, and M. Vauclin, *Journal of Physics D: Applied Physics* **31**, 1589 (1998).
- Z. Cai, X. Wang, B. Luo, W. Hong, L. Wu, and L. Li, *Composites Science and Technology* **145**, 105 (2017).
- K. C. Pitike and W. Hong, *Journal of Applied Physics* **115**, 044101 (2014).
- W. Hong and K. C. Pitike, *Procedia IUTAM* **12**, 73 (2015).
- H. Fröhlich, *Proceedings of the Royal Society of London. Series A, Mathematical and Physical Sciences* **160**, 230 (1937).
- E. Underwood, *Journal of microscopy* **89**, 161 (1969).
- A. R. C. Gerlt, R. S. Picard, A. E. Saurber, A. K. Criner, S. L. Semiatin, and E. J. Payton, *Metallurgical and Materials Transactions A* **49**, 4424 (2018).
- T. Bhimasankaram, S. V. Suryanarayana, and G. Prasad, *Current Science* **74**, 967 (1998).
- C.-W. Nan, *Physical Review B* **63**, 176201 (2001).
- Y. Sun, Z. Zhang, and C. P. Wong, *Polymer* **46**, 2297 (2005).
- G. Tarjus, P. Schaaf, and J. Talbot, *Journal of Statistical Physics* **63**, 167 (1991).
- A. R. West, D. C. Sinclair, and N. Hirose, *Journal of Electroceramics* **1**, 65 (1997).
- J. Y. Li, L. Zhang, and S. Ducharme, *Applied Physics Letters* **90**, 132901 (2007).
- E. Allahyarov, H. Lowen, and L. Zhu, *Physical Chemistry Chemical Physics* **18**, 19103 (2016).
- D.-H. Yoon, J. Zhang, and B. I. Lee, *Materials Research Bulletin* **38**, 765 (2003).
- T. Furukawa, K. Ishida, and E. Fukada, *Journal of Applied Physics* **50**, 4904 (1979).
- T. Yamada, *Journal of Applied Physics* **53**, 4328 (1982).
- R. W. Sillars, in *Institution of Electrical Engineers - Proceedings of the Wireless Section of the Institution; Vol. 12* (1937), p. 139.
- N. Jayasundere and B. V. Smith, *Journal of Applied Physics* **73**, 2462 (1993).

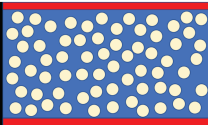
a)

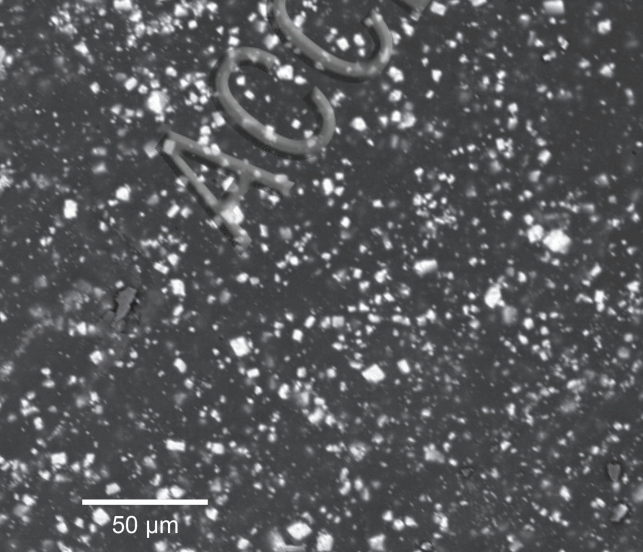


b)



c)





AACC



50 μm

